C103-E421

SHIMADZU
Excellence in Science

FTIR
TALK LETTER

Vol. 42

UEBAESOU is Japan's oldest artist paint store.
The solid paint they developed during the Meiji Period is still a popular product today.

Development of Dual Functional Catalytic Materials for CO_2 Capture and Selective Hydrogenation and Mechanistic Elucidation of High CO Selectivity Using FTIR Spectroscopy

Department of Environmental Chemistry and Chemical Engineering, School of Advanced Engineering, Kogakuin University

Maeno Zen, Associate Professor

1. Introduction

To reduce CO_2 emissions and establish a carbon-neutral society, demands for the development of new technologies for CO_2 capture and utilization are increasing. CO_2 adsorption and desorption using liquid and solid adsorbers, including amine- and zeolite-based materials, have been extensively studied. These systems are based on pressure and/or temperature swing operations, which are energy-intensive processes and require large-scale plants. Their targeted concentration is more than 10%, limiting their applicability for capturing lower-concentration CO_2. As an alternative strategy, CO_2 capture and reduction (CCR) with H_2 has recently attracted significant attention. Low-concentration CO_2 and H_2 gases are alternatively flowed in reactor systems through unsteady-state operations in which the captured CO_2 is converted to CH_4 and CO. For this, CO_2 adsorbers and CO_2 hydrogenation catalysts are combined regardless of whether the reactors are different or the same. In such cases, the operation temperatures for CO_2 capture and hydrogenation are often different. Dual functional materials (DFMs) with CO_2 capture and hydrogenation abilities have also gained considerable attention recently because they enable isothermal CCR. DFMs for CCR consist of alkaline (earth) metal oxides/carbonates and transition metal species, mainly group 8-10 metals, on metal oxide supports. Although various DFMs have been reported, most of them are aimed at CH_4 formation reactions [1]. On the other hand, there are only a few studies on catalysts that enable highly selective CO production [2]. In particular, there are no examples of CO synthesis by CCR from mixed gases including O_2 under mild conditions at ~300 °C, where direct utilization of exhaust gas is expected.

Recently, we developed the Na-promoted synthesis of Pt nanoparticles (NPs) on Al_2O_3 (Pt-Na/Al_2O_3) as an effective DFM for selective CO production through CCR. The developed catalyst was efficient under isothermal conditions at 350 °C. Comprehensive characterization revealed that the co-loaded Na species modified the Pt NPs, resulting in highly selective CO formation. Herein, we describe the CCR reaction systems with gas analysis using Fourier transform infrared (FTIR) spectroscopy as well as structural analysis and a plausible mechanism underlying the high selectivity of Pt-Na/Al_2O_3 based on comprehensive characterization, including in situ FTIR spectroscopy [3].

2. Preparation of Pt-based DFMs and Their CCR Performance Tests

Pt/Al_2O_3 and alkali/alkaline earth metal-modified Pt/Al_2O_3 [Pt–M/Al_2O_3 (M = Na, K, Mg, or Ca)] were synthesized by stepwise impregnation methods and their CO_2 capture performance from an O_2-containing mixture (1% CO_2/10% O_2/N_2) and successive reduction with H_2 (5% H_2/N_2) under isothermal conditions (350 °C) were investigated (Figure 1a). The uncaptured CO_2 and the generated CO and CH_4 were quantitatively analyzed from the peak area at 2395–2235, 2250–2001, and 3031–2994 cm^{-1}, respectively.

Pt/Al_2O_3 showed a low CO_2 absorption ability and afforded a small amount of CO and CH_4, with a CO selectivity of 11% (Figure 1b and c). In contrast, Pt-Na/Al_2O_3 exhibited a higher CO_2 absorption ability and yielded substantially more CO, with a much higher CO selectivity of 93%. Among the tested Pt-based DFMs, Pt-Na/Al_2O_3 afforded the highest CO production and selectivity. The concentration profiles of the effluent gas (Figure 1b) indicated a longer duration of CO_2 capture with Pt-Na/Al_2O_3 than with Pt/Al_2O_3 and Pt-Mg/Al_2O_3. During

the subsequent reduction in the presence of Pt/Al_2O_3 and $Pt\text{-}Mg/Al_2O_3$, the duration of CH_4 formation was longer (>300 s) than that of CO formation (50–150 s). In contrast, the duration of CO formation was much longer (>500 s) for $Pt\text{-}Na/Al_2O_3$, while CH_4 formation was continuously suppressed for durations >500 s. These results clearly demonstrate that the basic promoters influence the CO and CH_4 formation through the hydrogenation of the absorbed CO_2 with H_2.

(a)

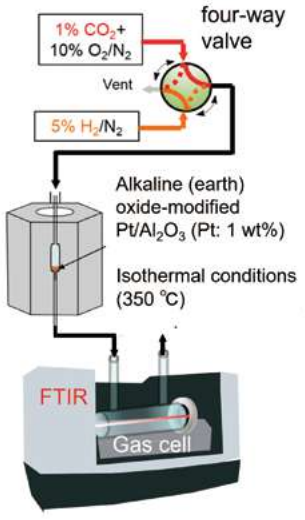

(b)

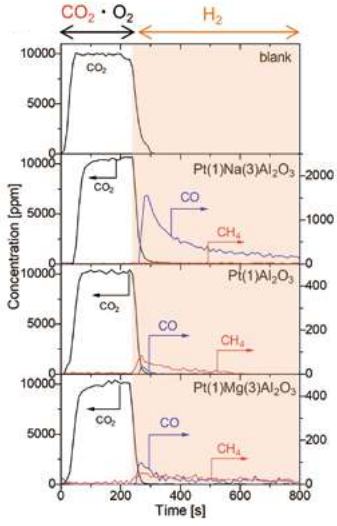

(c)

Dual functional material (DFM)	Max. CO Conc. [ppm]	CO formation [mmol/g]	CO Sel. [%]	CO_2 adsorption [mmol/g]	Conversion [%]
$Pt(1)/Al_2O_3$	37	0.001	11.1	0.08	9
$Pt(1)Na(3)/Al_2O_3$	1559	0.158	93.2	0.19	89
$Pt(1)K(6)/Al_2O_3$	57	0.007	31.1	0.12	19
$Pt(1)Mg(3)/Al_2O_3$	98	0.013	50.8	0.12	22
$Pt(1)Ca(6)/Al_2O_3$	310	0.041	84.1	1.07	5

Figure 1: CCR Using Pt-based DFMs: (a) Reaction and Analysis Systems Using FTIR Spectroscopy, (b) Concentration Profiles of Uncaptured CO_2 and Reduction Products (CO and CH_4) during CCR, and (c) Results of CCR Tests Using Pt-based DFMs

3. Characterization of $Pt\text{-}Na/Al_2O_3$ and Mechanistic Elucidation of the High CO Selectivity in CCR

Scanning transmission electron microscope (STEM) and energy-dispersive X-ray (EDX) analyses of $Pt\text{-}Na/Al_2O_3$ revealed that the Pt NPs were surrounded by Na species (Figure 2a). Line scan analysis showed that Pt atoms were in the core region, whereas Na atoms preferentially existed in the shell region, indicating the formation of core–shell-like NPs (Figure 2b). In contrast, the modified Pt NPs were barely observed in the elemental mapping images of $Pt\text{-}Mg/Al_2O_3$. To investigate the surface structure of the Pt NPs, FTIR spectroscopy of the CO species adsorbed on Pt/Al_2O_3 and $Pt\text{-}Na/Al_2O_3$ was performed (Figure 2c). For Pt/Al_2O_3, the two small peaks at 2102 and 2082 cm^{-1} were derived from the on-top CO adsorbed on the terrace-like sites of the Pt NPs (corresponding to well-coordinated Pt sites), while the main band at ~2065 cm^{-1} was derived from the on-top CO on the step-like sites of the Pt NPs (under-coordinated Pt sites). For $Pt\text{-}Na/Al_2O_3$, the peak corresponding to the terrace-like sites was hardly observed. These observations strongly suggest that the Pt NPs were modified with the Na species (Figure 2d).

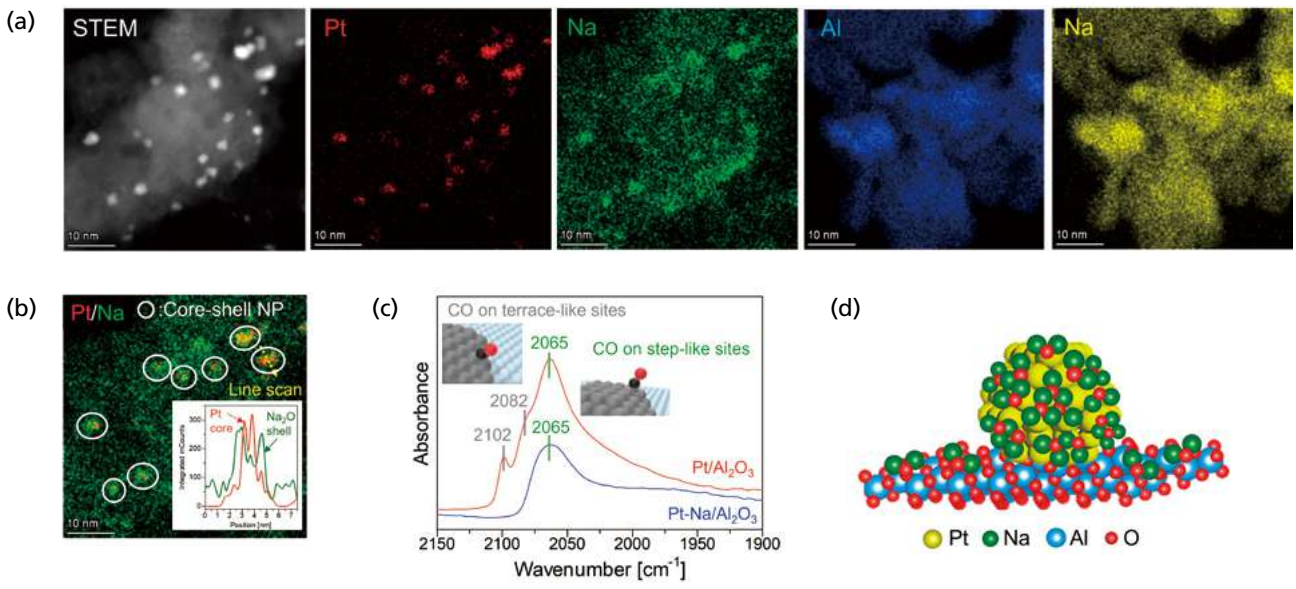

Figure 2: Characterization of Pt-Na/Al_2O_3: (a) STEM and EDX Mapping of Pt-Na/Al_2O_3, (b) Line Scan Analysis of Na-modified Pt NPs, (c) FTIR Spectra of the Adsorbed CO on Pt/Al_2O_3 and Pt-Na/Al_2O_3, and (d) Possible Structure of Pt-Na/Al_2O_3.

To elucidate the high selectivity of Pt-Na/Al_2O_3, in situ FTIR spectroscopy was carried out during CCR (Figure 3a). Prior to the experiment, self-supported disks were placed in a quartz cell and treated with H_2 at 350 °C. Background spectra were obtained under N_2 flow, without exposure to air. For Pt/Al_2O_3, the two peaks at 1587 and 1341 cm^{-1} appearing during CO_2 capture could be assigned to the absorbed CO_2, possibly existing as monodentate CO_3^{2-}. After the flow gas was changed from 1% CO_2/10% O_2/N_2 to 5% H_2/N_2 (t = 0 min), the intensity of the two peaks decreased and a new peak derived from the on-top CO on metallic Pt was observed at 2048 cm^{-1}. When Pt-Na/Al_2O_3 was used instead of Pt/Al_2O_3, much more intense peaks derived from CO_3^{2-} were observed during CO_2 capture, confirming the enhanced CO_2 absorption ability (Figure 3b). Notably, during the successive reduction, the on-top CO species was hardly observed whereas the peak intensities for the adsorbed CO_3^{2-} continuously decreased (Figure 3b). Based on these results, the high efficiency of Pt-Na/Al_2O_3 can be explained as follows. The Na species on the Pt NPs served as CO_2 capture sites adjacent to the Pt NPs, where the absorbed CO_2 species were efficiently reduced by H_2. In addition, adsorption of the generated CO was effectively inhibited because the surface of the Pt NPs was modified by the Na species, suppressing the successive reduction of CO to CH_4 (Figure 3c).

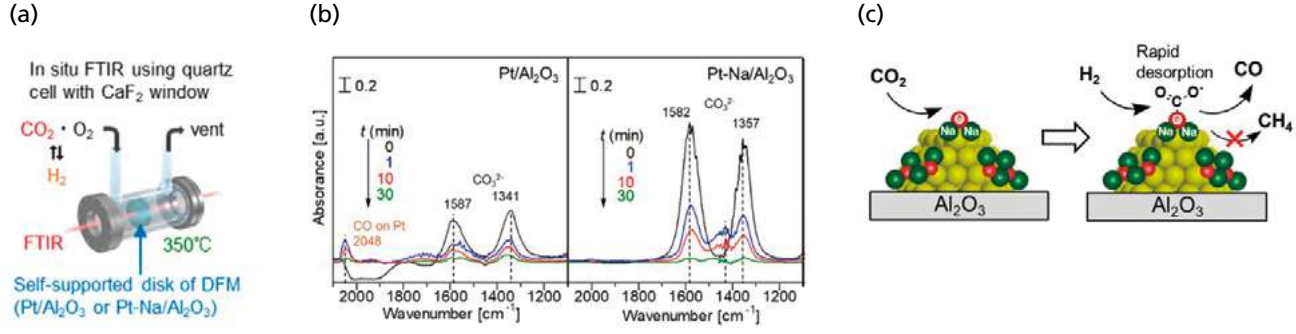

Figure 3: In Situ FTIR Spectroscopy of the Surface-adsorbed Species on DFMs During CCR:
(a) In Situ FTIR Spectral Measurement System,
(b) In Situ FTIR Spectra during CCR for (left) Pt/Al_2O_3 and (right) Pt-Na/Al_2O_3,
and (c) Plausible Mechanism of the Highly Selective CO Formation over Pt-Na/Al_2O_3.

4. Summary

This study successfully developed Pt-Na/Al_2O_3 as an effective DFM for selective CO formation through CCR at a mild temperature (350 °C). The Na-modified Pt NPs were formed in Pt-Na/Al_2O_3, as revealed by STEM, EDX elemental mapping, and FTIR spectroscopy with CO adsorption experiments. We also conducted in situ FTIR spectroscopy during CCR, in which the adsorbed CO species were hardly observed over Pt-Na/Al_2O_3. The Na species on the Pt NPs not only served as CO_2 absorption sites but also suppressed the adsorption of the generated CO, leading to highly selective CO production. These results reveal the effect of basic promoters on the surface structures of metal NPs and product selectivity, demonstrating the importance of the choice and loading of basic promoters during the development of DFMs for CCR. Notably, the optimized Pt-Na/Al_2O_3 was applicable for continuous CCR operation, where the CO_2 capture capacity and CO productivity were maintained for at least 6000 cycles [3]. We have also recently developed non-noble metal-based DFMs effective for CO and CH_4 formation [4,5] as well as a combined system capable of direct air capture and CCR [6].

The study reported herein was performed in Hokkaido University, Institute for Catalysis (former institute), under the supervision of Prof. Ken-ichi Shimizu. We are sincerely grateful to all members and corroborating researchers for their guidance and cooperation in conducting this research.

References

[1] M. S. Duyar, M. A. A. Treviño, R. J. Farrauto, Appl. Catal. B Environ, 2015, 168-169, 370; F. Kosaka, T. Sasayama, Y. Liu, S.-Y. Chen, T. Mochizuki, K. Matsuoka, A. Urakawa, K. Kuramoto, Chem. Eng. J., 2022, 450, 138055.

[2] L. F. Bobadilla, J. M. Riesco-García, G. Penelás-Pérez, A. Urakawa, J. CO2 Util., 2016, 14, 106.

[3] L. Li, S. Miyazaki, S. Yasumura, K. W. Ting, T. Toyao, Z. Maeno K. Shimizu, ACS Catal., 2022, 12, 2639.

[4] L. Li, Z. Wu, S. Miyazaki, T. Toyao, Z. Maeno, K. Shimizu, RSC Adv., 2023, 13, 2213.

[5] L. Li, N. Zhang, Z. Wu, S. Miyazaki, T. Toyao, Z. Maeno, K. Shimizu, Chem. Eng. J., 2023, 477, 147199.

[6] L. Li, S. Miyazaki, Z. Wu, T. Toyao, R. Selyanchyn, Z. Maeno, S. Fujikawa, K. Shimizu, App. Catal. B, 2023, 339, 123151.

Configuration of the AIRsight Infrared Raman Microscope

Spectroscopy Business Unit, Analytical & Measuring Instruments Division
Ryuta Shibutani

Shimadzu released the AIRsight infrared/Raman microscope on November 16, 2022. This product is the only widely-used microscope in the world that enables analysis with two analytical methods, infrared spectroscopy and Raman spectroscopy, in the same system. By adding a Raman unit to an existing infrared microscope, it enables both infrared and Raman measurements. This article describes the internal modifications that enable both measurement mechanisms to be included within the same instrument.

1. Introduction

First, the following lists some of the benefits of analyzing samples with two different analytical methods, infrared spectroscopy and Raman spectroscopy, in the same system.

Same position
is measured by IR and Raman

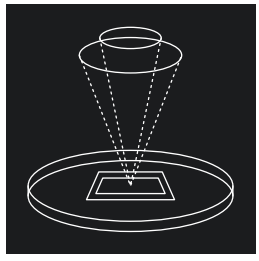

Measure the Same Position by Both Infrared and Raman Spectroscopy without Moving the Sample

Both infrared and Raman spectra can be measured from the same location in an extremely small area without moving the sample. In addition to ease of use, this significantly improves the accuracy of qualitative analysis by providing information about both organic and inorganic matter in the same location.

Single system
saves space

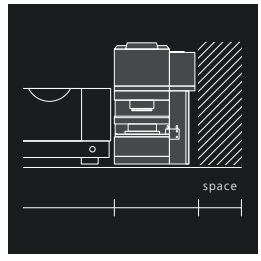

Organic and Inorganic Information Obtainable with One Instrument

A single AIRsight unit can analyze mixtures of both organic and inorganic substances. It also helps save space, because a single system serves the role of both infrared and Raman microscopes.

Smart software
controls IR and Raman

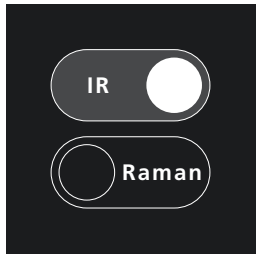

Measure/Analyze Both Infrared and Raman Spectra with the Same Software Program

The AMsolution control software enables easy switching between infrared or Raman measurement/analysis modes with a single click. It also can display acquired infrared and Raman spectra overlaid.

The following describes the respective characteristics in more detail.

2. Same Position

The following five sample observation/measurement methods can be selected in AIRsight.

	Application	Camera, Objective Mirror, and Objective Lens	Mode	Field of View
1	Observation	Wide-view camera	Infrared/Raman	Max. 10 × 13 mm
2	Observation/measurement	15× reflecting objective mirror	Infrared	Min. 30 × 40 µm
3		High-sensitivity reflecting objective mirror (GAO)		
4		50× objective lens	Raman	Min. 15 × 20 µm
5		100× objective lens		Min. 7.5 × 10 µm

First, the wide-field camera is used to determine the approximate measurement position by viewing a large area. Next, the microscope is switched to the objective mirror mode for infrared observation/measurements or the objective lens mode for Raman observation/measurements to view a smaller area and decide the measurement points. In the infrared mode, the zoom level can be increased to a maximum 330× magnification using the wide-field camera in combination with the 15× reflecting objective mirror (refer to Figure 1). In the Raman mode, the zoom level can be increased to a maximum 660× or 1,330× magnification using the wide-field camera in combination with the 50× or 100× objective lens. Note that the infrared 15× reflecting objective mirror and Raman 50×/100× objective lens can be mounted at the same time and up to five types of cameras, objective mirrors, or objective lens can be installed in the revolver (refer to Figure 2).

Because the same positional information is shared for the wide-field camera, infrared 15× reflecting objective mirror, and Raman objective mirror, there are no positional shifts when switching between camera modes. Positional information is also shared when switching between the infrared and Raman modes. That eliminates the need to search for measurement points again when switching to a different measurement mode after measurement was performed in the infrared or Raman mode.

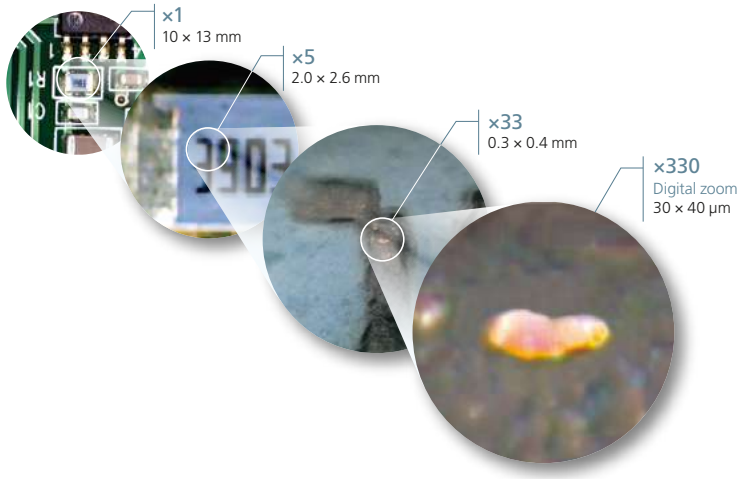

Figure 1: Zoom Function Using the Wide-Field Camera in Combination with the 15× Reflecting Objective Mirror for Infrared Measurements

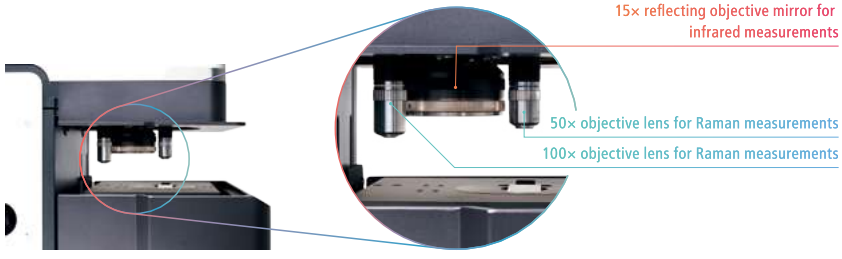

Figure 2: 15× Reflecting Objective Mirror for Infrared Measurements and Objective Lens for Raman Measurements Mounted on the Revolver (Max. five types can be mounted simultaneously)

3. Smart Software

The measurement mode can be switched easily between infrared (IR) and Raman modes with a single click of a button at the top of the AMsolution software window (refer to Figure 3).

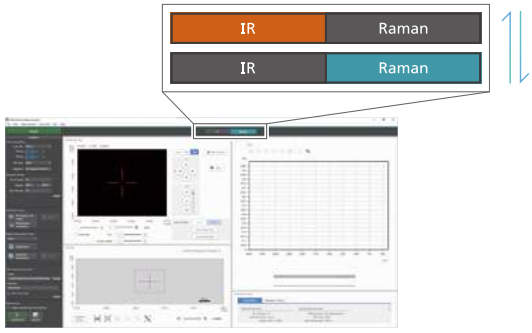

Figure 3: Mode Switching Buttons (shown with the IR mode selected above or Raman mode selected below)

Furthermore, AMsolution software is designed with minimal user interface differences between infrared and Raman modes, achieving an operating feel that is as similar as possible. That means operating methods learned for one mode can be used to operate the microscope in the other mode without having to refer to the instruction manual or other documentation.

4. Single System

The AIRsight has about the same installation footprint size as an AIMsight infrared microscope, but is slightly larger in the depth direction due to the laser unit located at the back of the system. However, it requires far less space than if 2 units, both an infrared microscope and a Raman microscope, were installed. Note that because the AIRsight uses a laser, it includes a cover near the stage that can be opened/closed to ensure operator safety by blocking the laser light. The system is also designed to prevent laser oscillation if the laser cover is not closed.

In addition, in order to minimize installation space, the AIRsight uses some optical elements for both Raman and infrared optics.

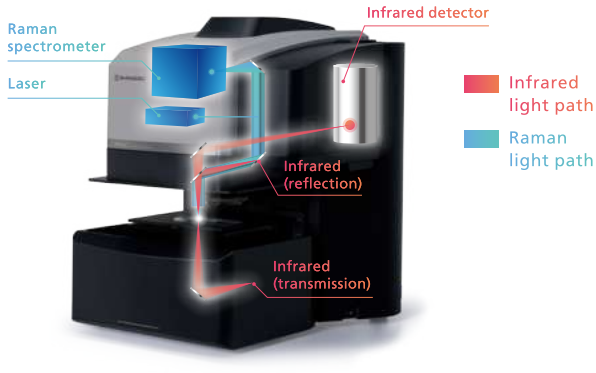

Figure 4: Illustration of Infrared and Raman Light Paths

Key shared elements include the visible lighting, revolver, and mirrors. The revolver and mirrors are described in more detail below.

Revolver

Up to five types of objective lens, mirror, or wide-field camera elements can be mounted on the revolver, as shown in Figure 2. The revolver can be rotated up to 239 degrees. Because the wide-field camera is connected via a wired cable, rotating the revolver can pull out the cable or leave extra slack. Therefore, a cable winding mechanism is included on top of the revolver for adjusting the wide-field camera cable length.

Mirrors

Switching between pathways for infrared transmission, infrared reflection, and Raman measurements is achieved by varying the angle of mirrors inside the instrument. The following describes the switching mechanism in more detail.

There are three mirrors inside the AIRsight unit for switching between the optical paths. The first mirror, which is also included in conventional infrared microscopes, switches between infrared transmission and infrared reflection (transmission/reflection switching mirror in Figure 5). It is positioned upstream in the infrared optical path to switch the infrared optical path.

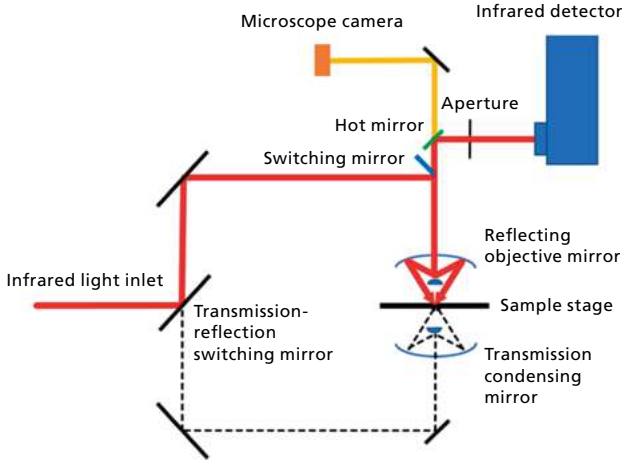

Figure 5: Optical System for Infrared Measurements

The second mirror is a half-mirror used to switch between infrared and Raman optical paths. During observations and infrared measurements in the infrared mode, the half-mirror rotates and moves toward the back, as shown in Figure 6. During observations and Raman measurements in the Raman mode, the half-mirror rotates for use in visible light and infrared optical paths. That results in the laser light for Raman measurements and the Raman scattering from samples using the same optical path as for infrared measurements (refer to Figure 6).

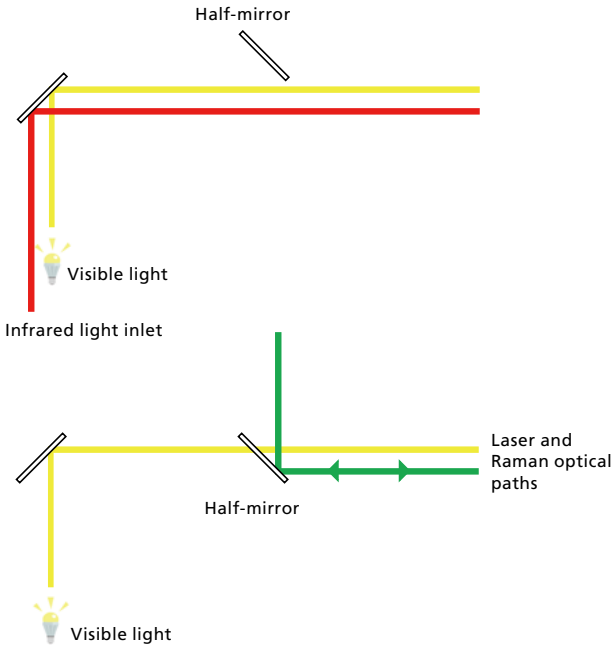

Figure 6: Half-Mirror for Switching between Infrared and Raman Measurement Modes

The third mirror is a switching mirror positioned directly above the revolver (switching mirrors in Figure 5 and 7). It moves away from the optical path during infrared transmission measurements, moves to the edge mirror position during infrared reflection measurements (with the mirror reflecting half of the optical path), and rotates to the full-reflection position during Raman measurements (Figure 8).

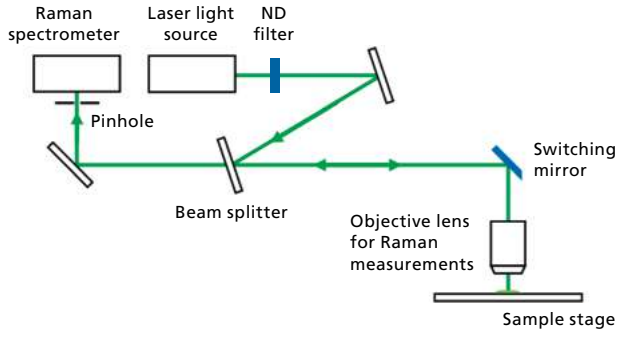

Figure 7: Optical System during Raman Measurements

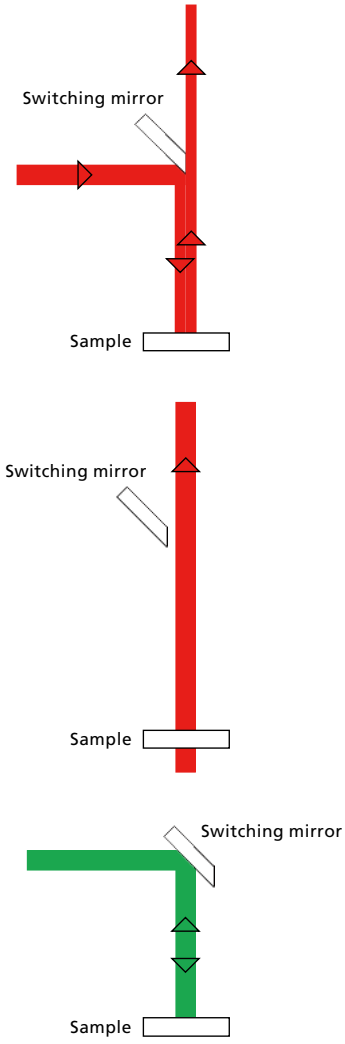

Figure 8: Switching Mirror Positions during Infrared and Raman Measurements
(Upper: Infrared Reflection Measurements;
Center: Infrared Transmission Measurements;
Lower: Raman Measurements)

Using the same revolver and mirrors for both measurement modes, as described above, enabled the development of a more compact infrared/Raman microscope. To improve operability, mode switching buttons located at the top of all AMsolution software windows can be pressed to automatically switch between those respective revolver and mirror positions.

5. Conclusion

This article describes key features and internal mechanisms of the AIRsight microscope. Readers are urged to try an actual AIRsight microscope in order to fully experience the superior operability and compact size.

Notes on Infrared Spectral Analysis – Aliphatic Saturated Hydrocarbons (Paraffins) –

Solutions Center of Excellence, Analytical & Measuring Instruments Division
Yoshiyuki Tange, Yasushi Suzuki

A previous article (FTIR TALK LETTER Vol. 41) provided introductory notes on infrared spectroscopy, including the vertical axis of infrared spectra, the fundamental vibrations of molecules, and the characteristic absorption bands of common functional groups. This article includes notes on infrared spectral analysis of aliphatic saturated hydrocarbons (paraffins), including polyethylene (PE) and polypropylene (PP), two of the most basic organic substances and commonly known as general-purpose plastics. The notes on data analysis include not only information about distinguishing between PE and PP, but also describe a technique that can be used to distinguish between the different crystallization (density) levels in PE materials. This article also briefly discusses molecular vibration modes that affect the orientation of molecules in PP.

1. Using Infrared Spectra to Classify Paraffins

First, Figure 1 shows the main peak positions of hydrocarbons composed of only carbons and hydrogens and provides an example of their classification method. The three types of hydrocarbons (paraffins, olefins, and aromatics) can be easily classified by successively checking for the presence of corresponding peaks, starting from the high-wavenumber end of the spectrum and moving toward the low-wavenumber end.

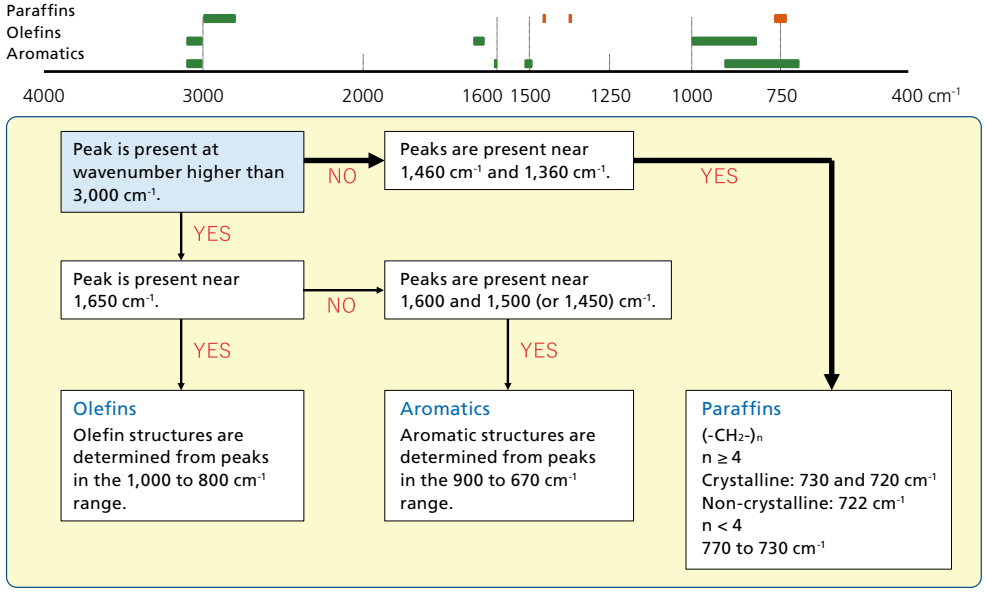

Figure 1: Infrared Spectral Peak Positions and Classification Flow Chart for Paraffin

The next section provides notes on analyzing the peaks that appear in respective wavenumber regions. The first note is about the peaks from C-H stretching vibration that appear near 3,000 cm^{-1}. Figure 2 shows the peaks near 3,000 cm^{-1} for typical paraffins, olefins, and aromatics.

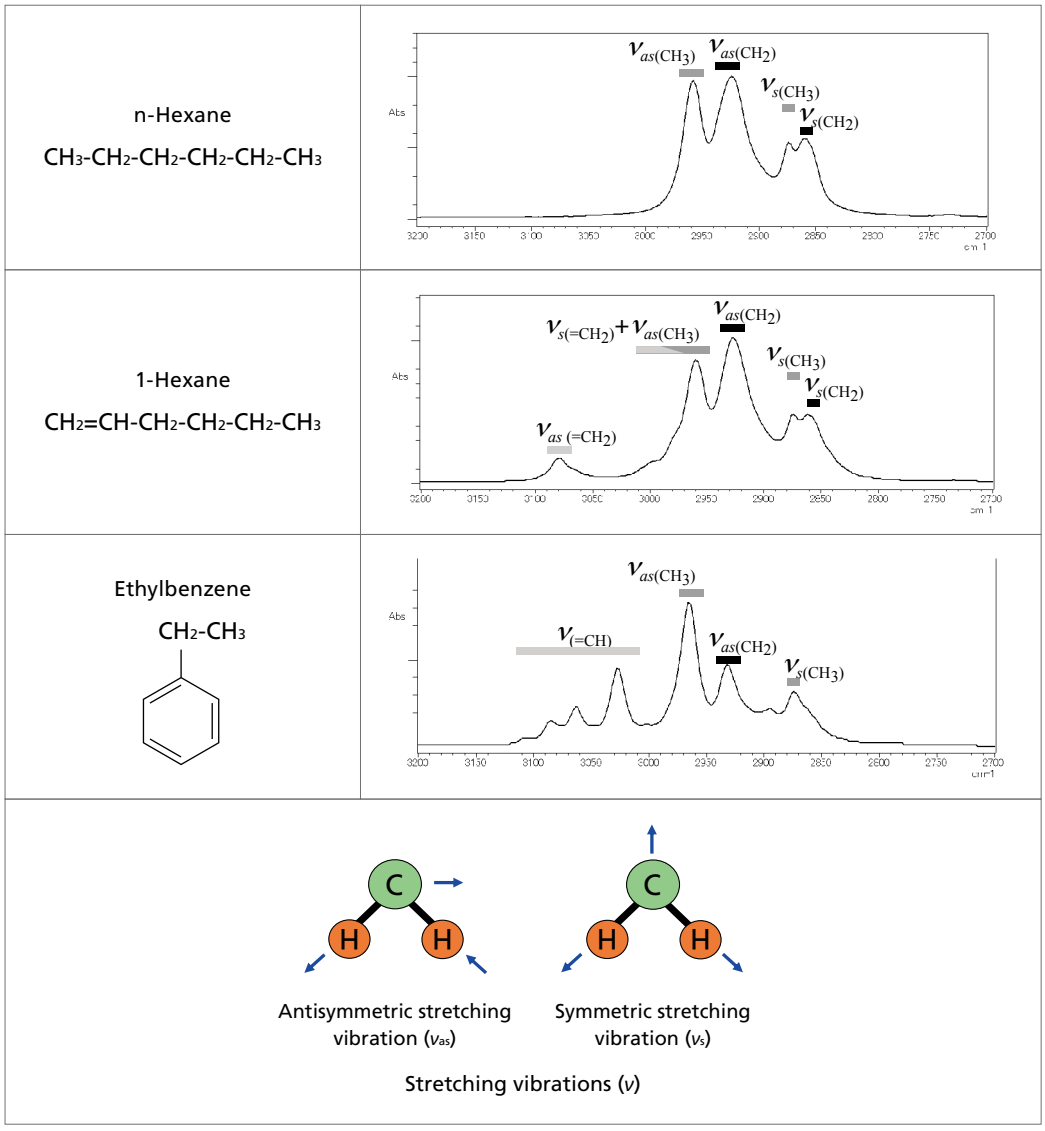

Figure 2: Attribution of Peaks Near 3,000 cm^{-1} [1]

Peaks near the 3,000 to 2,800 cm^{-1} range are caused by C-H stretching vibration and appear for all paraffins, olefins, and aromatics. In contrast, if a double or triple bond is present between the C-H hydrogen and an adjacent carbon, such as in -C=C-H or -C≡C-H structures, then the C-H stretching vibration appears in a higher wavenumber region above 3,000 cm^{-1}. Because paraffins contain only single-bonded carbons, they generate no C-H stretching vibration peaks in a wavenumber region above 3,000 cm^{-1}, but olefins and aromatics include -C=C-H or -C≡C-H structures that result in multiple peaks near the 3,000 cm^{-1} wavenumber due to C-H stretching vibration. Thus, it is possible to distinguish between paraffins, olefins, and aromatics by checking for the presence of C-H stretching vibration peaks above 3,000 cm^{-1}.

Focusing only on paraffins, the following describes the peaks near 1,460 cm^{-1} and 1,360 cm^{-1} caused by CH_2 scissoring vibration and CH_3 deformation vibration. Figure 3 shows PE and PP spectra near 1,500 to 1,300 cm^{-1}.

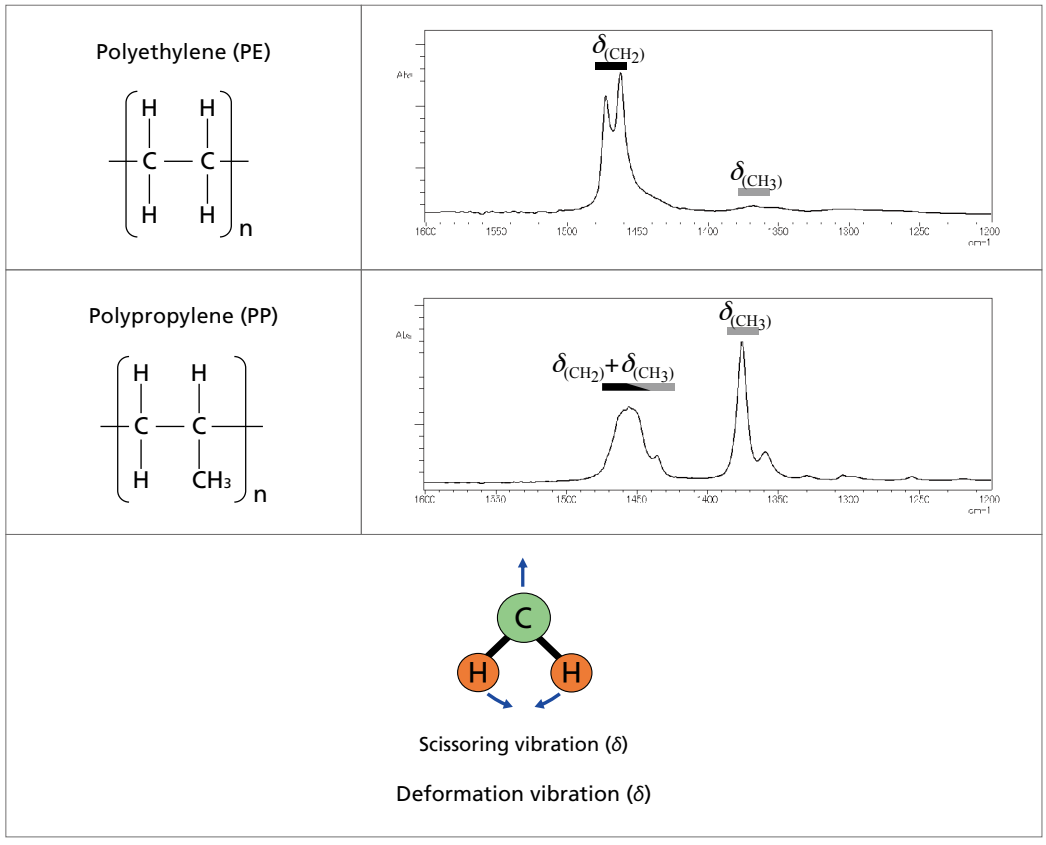

Figure 3: Attribution of Peaks Near 1,460 cm^{-1} and 1,360 cm^{-1} [1]

The peaks near 1,460 cm^{-1} and 1,360 cm^{-1} are caused by CH_2 scissoring vibration and CH_3 deformation vibration. Paraffins are mainly composed of methylene (CH_2) and methyl (CH_3) groups, with differences in the ratio of methylene and methyl groups being based on the compound. Whereas the PE structure consists of a straight chain of methylene groups, the PP structure includes a methyl group in place of one of the hydrogens in the PE structure. (Refer to the structural formulas in Figure 3.) When checking infrared spectra, PP will exhibit more peaks from methyl groups than PE.

The following describes the peaks near 750 cm^{-1} caused by CH_2 rocking vibration. Figure 4 shows PE, 1-propanol, and ethanol infrared spectra near 800 to 500 cm^{-1}.

The peak positions caused by CH_2 rocking vibration shown here are useful for estimating the length of carbon chains. If the length of the methylene group is expressed as $(CH_2)n$, then the wavenumber position where the peaks appear will differ depending on the number of methylene groups. If the carbon number due to the methylene groups is $n \geq 4$, then the peaks will appear in the 720 to 725 cm^{-1} region. For 1-propanol with $n = 2$, a CH_2 rocking vibration peak appears on the broad peak for C-O-H deformation vibration, but this shows that the peak appears at a wavenumber higher than 750 cm^{-1}. For ethanol with $n = 1$, no CH_2 rocking vibration peak appears. However, slight CH_2 rocking vibration may be detected in some cases for copolymers of PP and PE.

The 4,000 to 400 cm^{-1} infrared spectra of PE and PP are shown in Figure 5 and criteria for distinguishing between PE and PP are summarized on page 14.

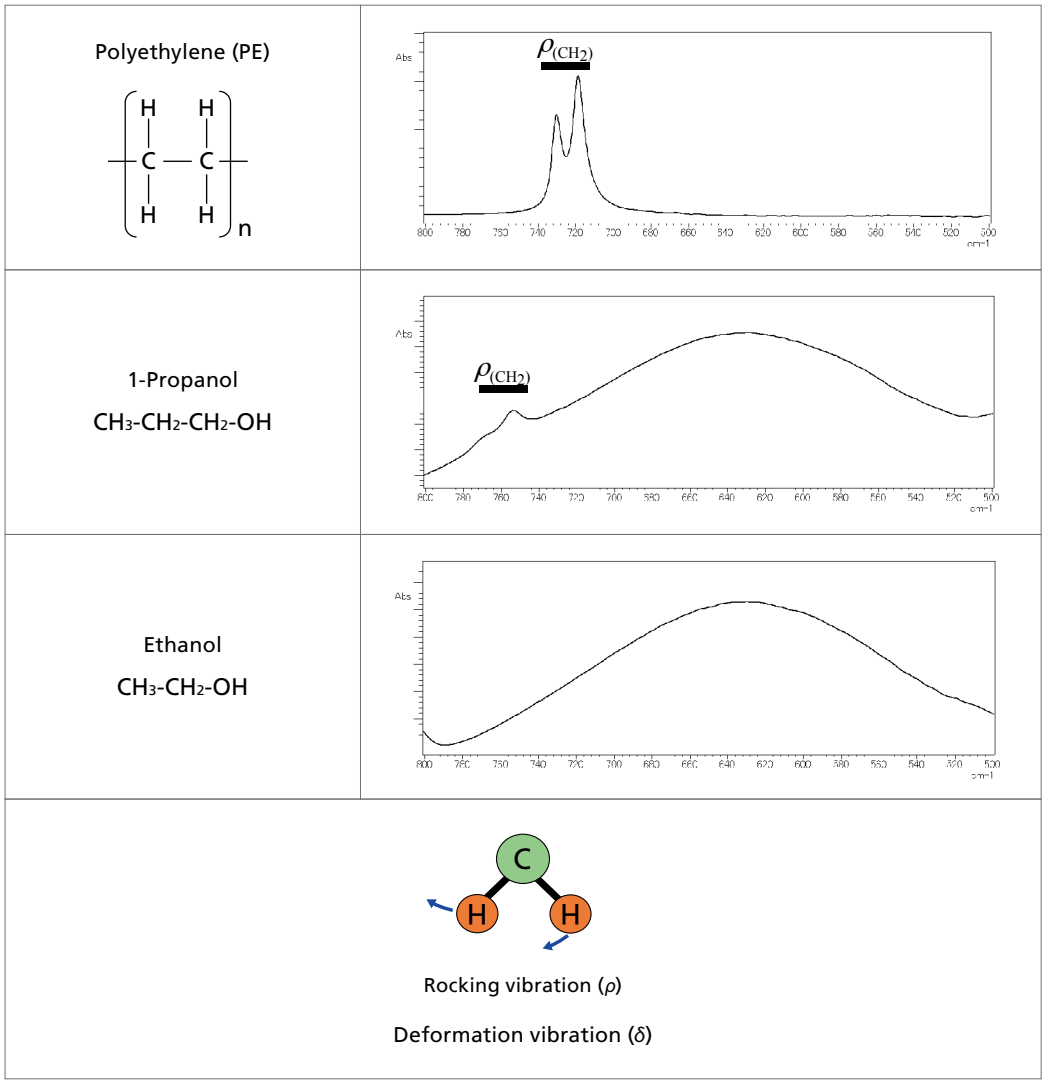

Figure 4: Attribution of Peaks Near 750 cm^{-1} [1]

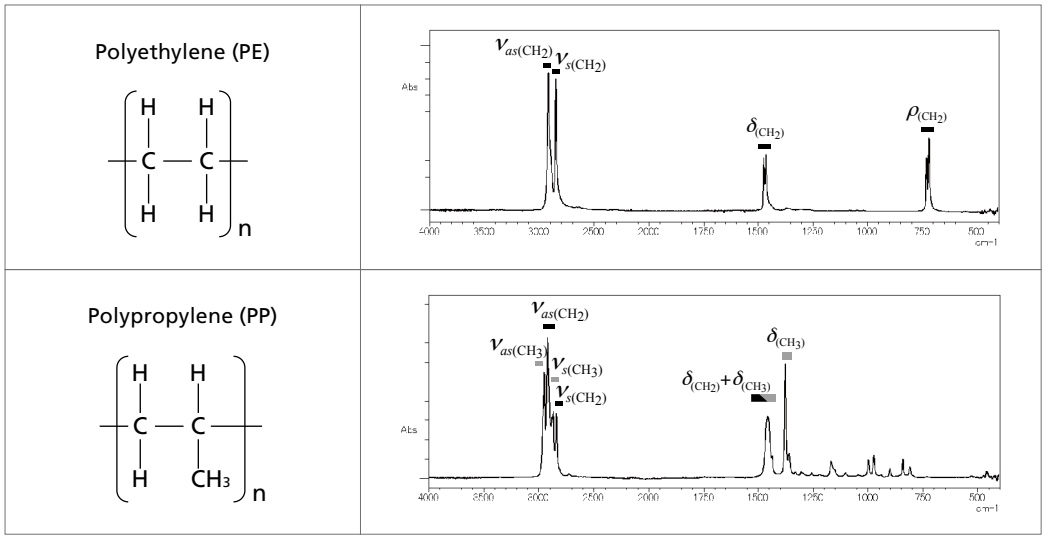

Figure 5: Infrared Spectra of PE and PP (Entire) [1]

Main Differences between PE and PP Spectra

- **Peaks from Methyl Groups**
  PE only includes two methyl groups on the ends, so almost no peaks from methyl groups, or only very slight peaks, appear in PE infrared spectra.
- **Peaks from CH_2 Rocking Vibration**
  PP structures include almost no methylene group chains, so almost none of the peaks from CH_2 rocking vibration appear in infrared spectra.

2. Crystallinity (Density) Differences in PE and Molecular Vibration Modes in PP that Affect Molecular Orientation

Even for compounds that are identical if expressed as a structural formula, differences in crystallinity (density) or orientation can result in different hardness or viscosity properties. The following describes how to distinguish between PE materials with different crystallinity (density) and the relationship between PP orientation and molecular vibration.

Crystallinity (Density) Differences in PE –High vs Low Density PE–

High-density polyethylene (HDPE) and low-density polyethylene (LDPE) materials can have different stretchiness, gas permeability, transparency, and other properties. Therefore, their selection depends on application objectives.

In terms of molecular structure, HDPE has fewer side chains, whereas LDPE molecules are less prone to blockage, due to a greater number of longer side chains (refer to Figure 6).

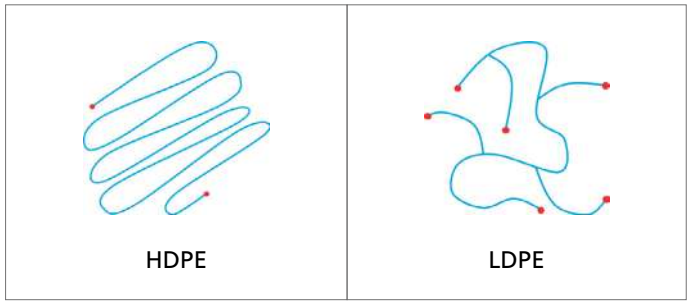

Figure 6: Structures of HDPE and LDPE (Illustrative Image)

Figure 7 shows an overlay of HDPE and LDPE infrared transmission spectra in the 1,600 to 1,200 cm^{-1} region.

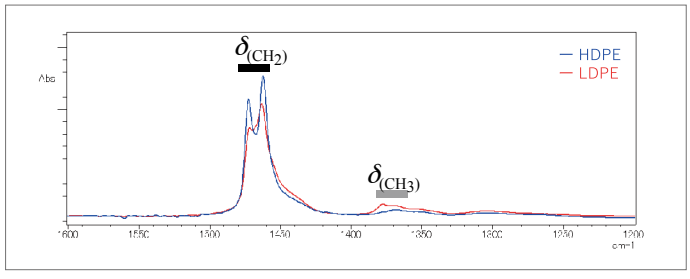

Figure 7: Overlay of HDPE and LDPE Infrared Spectra (Transmission Method)

LDPE includes a methyl group on the end of methylene group carbon chains (indicated as red dots in the LDPE structure in Figure 6). Compared to HDPE, that results in weaker absorption by the methyl groups, as shown in Figure 7 (indicated as $\delta(CH_3)$ in Figure 7). In contrast, high-density HDPE includes more methylene groups than LDPE, which results in relatively stronger CH_2 scissoring vibration (indicated as $\delta(CH_2)$ in Figure 7). For more details, refer to Application News 01-00710 about using infrared spectra to distinguish between PE and PP materials.

Molecular Vibration Modes in PP that Affect Molecular Orientation

The molecule orientation of compounds can determine the dimensional stability and strength in specific directions. A check of the PP infrared spectrum in Figure 5 reveals multiple unattributed peaks near the 1,300 to 800 cm^{-1} region. Those peaks are mainly caused by a mixture of molecular vibrations. Though it would be difficult to use those peaks for qualitative identification of compounds, the corresponding vibration has an orientation that can be used to investigate molecular orientation.

Figure 8 shows an example of measuring a PP string material in the transversely polarized light and axially polarized light.

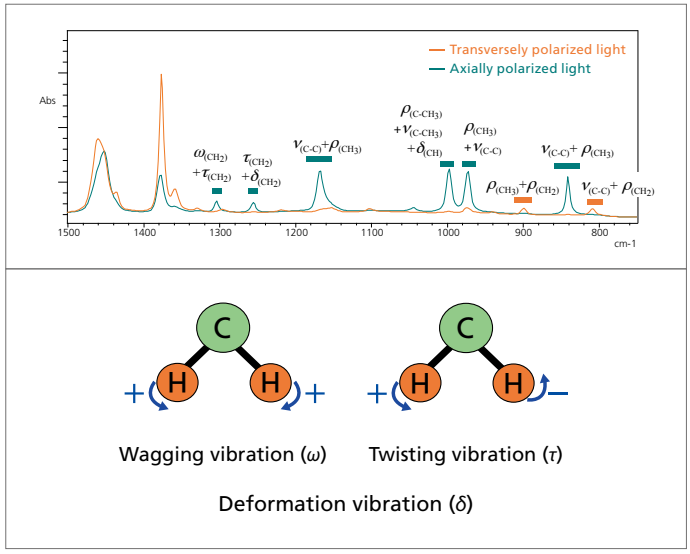

Figure 8: Polarized Light Measurements (Transmission Method) of PP String Material [2]

PP string material used for tying packages has high tensile strength in the axial direction, but can be easily ripped with fingers in the transverse direction. Therefore, it is predicted to have an axial molecular orientation. The infrared spectrum measured with axially polarized light (green line) detected strong CH_2 wagging vibration and CH_2 twisting vibration at 1,304 cm^{-1}, CH_2 twisting vibration and C-H deformation vibration at 1,256 cm^{-1}, C-C stretching vibration and CH_3 rocking vibration in two locations (at 1,168 cm^{-1} and 841 cm^{-1}), and other results. In contrast, the infrared spectrum measured with transversely polarized light (orange line) detected strong CH_3 rocking vibration and CH_2 rocking vibration at 899 cm^{-1}, C-C stretching vibration and CH_2 rocking vibration at 809 cm^{-1}, and other results. That means if the molecular vibration levels parallel and perpendicular to the molecular orientation are known, polarized light measurements can be used to investigate molecular orientation. In addition to macro-scale evaluations, polarized light measurements could also be used in combination with infrared microscope measurements for micro-scale investigations of in-plane molecular orientations.

3. Conclusion

The key points about infrared spectral analysis noted in this article are summarized below.

- Paraffins, olefins, and aromatics can be identified by checking for the presence of C-H stretching vibration peaks in a wavenumber region above 3,000 cm^{-1}.
- To determine the number of methyl groups, look for CH_3 deformation vibration peaks at 1,360 cm^{-1}. Those peaks can be used to distinguish between PE and PP or between LDPE and HDPE.
- To determine the number of methylene groups, look for CH_2 rocking vibration peaks at 750 cm^{-1}. Those peaks can be used to distinguish between PE and PP.
- Even if peaks cannot be used for qualitative analysis of compounds, they might provide information about molecular orientation. The next article will feature notes on analyzing unsaturated hydrocarbons, such as olefins and aromatics.

References

[1] Shigeyuki Tanaka, Norio Teramae, Infrared Spectroscopy, Kyoritsu Shuppan (1993)

[2] Koichi Nishikida, Etsuo Nishio, Chart-Based FT-IR Analysis, Kodansha Scientific Ltd. (1990)

Fourier Transform Infrared Spectrophotometer

NEW IRSpirit-X Series

IRSpirit, Ready to Run

Space-Saving, Expandable

- Great for Small Lab Spaces
- Standard-Sized Sample Compartment in a Compact Bench

FTIR Made Easier

- IR Pilot Pre-built Macro Program
- Spectrum Advisor Function
- Contaminant Analysis Program
- Identification Test Program

Reliability to Deploy with Confidence

- Internal Dehumidifier (Optional) Ensures Robustness
- Reliable Parts Come with a 10-Year Warranty

Note: This warranty does not cover consumables, accessories other than the FTIR main unit, PCs and peripherals, instruction manuals, jigs, and labor charges for the second and subsequent years.

Reliable parts
10 YEARS
WARRANTY

Simple Operation, Confident Results

- Acquisition and Analysis of EDX and FTIR Data from a Single Computer

IRSpirit-X Series
Product Information

SHIMADZU

Shimadzu Corporation
www.shimadzu.com/an/